Clays and Clay Minerals, Vol. 39, No. 4, 387–399, 1991.

EFFECTS OF OCTAHEDRAL Mg^{2+} AND Fe^{3+} SUBSTITUTIONS ON HYDROTHERMAL ILLITIZATION REACTIONS

NECIP GÜVEN

Department of Geosciences, Texas Tech University, P.O. Box 4109
Lubbock, Texas 79409

WUU-LIANG HUANG

Exxon Production Research Company, Houston, Texas 77001

Abstract—Three gels of illitic composition having different octahedral substitutions were hydrothermally treated in distilled water at 300°C and 500 bars for 7 to 90 days. The gel of the composition $K_{0.7}Al_{2.0}(Si_{3.3}Al_{0.7})O_{10}(OH)_2$, having no octahedral substitutions, yielded poorly crystalline and randomly interstratified illite/smectite (I/S) having possibly 30% or more expandability. These I/S particles occurred predominantly as foliated or compact lamellar aggregates having morphological features characteristic of common smectite. Laths having a morphology similar to that of diagenetic "fibrous illites" were also found in small amounts after the gel had been aged for 35 days. Their chemical composition was similar to that of the foliated aggregates of I/S in the same run.

Illitic gel having the composition $K_{0.7}(Al_{1.7}Fe^{3+}_{0.3})(Si_{3.3}Al_{0.7})O_{10}(OH)_2$ having octahedral Fe^{3+} substitutions yielded more and better crystalline I/S. The reaction products of the 7–35-day runs consisted mainly of randomly interstratified I/S having an expandability of 90 to 65%. The I/S particles occurred as foliated or compact lamellar aggregates having a smectite-like morphology, as described above. The Fe^{3+}-bearing gel yielded, after 90 days of ageing, an R1-ordered I/S having 25% expandability and a morphology of ribbons and hexagonal platelets.

Illitic gel of composition $K_{0.8}(Al_{1.6}Mg_{0.4})(Si_{3.6}Al_{0.4})O_{10}(OH)_2$ having octahedral Mg^{2+} substitutions produced no illite even after 90 days of ageing, but a pure smectite in the form of foliated aggregates.

Key Words—Illite/smectite, Illitization, Interstratification, Octahedral substitution, Synthesis.

INTRODUCTION

The effects of interlayer cations, such as Na^+, K^+, Ca^{2+}, and Mg^{2+}, on the hydrothermal crystallization of illite have been well established by numerous studies (e.g., Eberl, 1978a, 1978b; Eberl and Hower, 1977; Roberson and Lahann, 1981; Inoue, 1983; Whitney and Northrop, 1988). These studies demonstrated the paramount importance of K^+ in illitization reactions.

The possible effects of octahedral substitutions, especially Mg^{2+} and Fe^{3+}, in illite structures have so far drawn very little attention regarding the hydrothermal crystallization kinetics and the morphological and structural evolution of illites. To evaluate these effects, glasses of illitic compositions containing Mg^{2+} and Fe^{3+} octahedral substitutions were prepared and hydrothermally treated. The hydrothermal experiments and their reaction products are described in the following.

EXPERIMENTAL PROCEDURES

Gels having chemical compositions corresponding to the following structural formulae of illite were prepared:

Gel I (with no Mg^{2+} and Fe^{3+} substitutions):
$K_{0.7}Al_{2.0}(Si_{3.3}Al_{0.7})O_{10}(OH)_2$

Gel II (with Fe^{3+} substitutions):
$K_{0.7}(Al_{1.7}Fe^{3+}_{0.3})(Si_{3.3}Al_{0.7})O_{10}(OH)_2$

Gel III (with Mg^{2+} substitutions):
$K_{0.8}(Al_{1.6}Mg_{0.4})(Si_{3.6}Al_{0.4})O_{10}(OH)_2$

These gels were hydrothermally aged in distilled water at a 1:1 solid/water mass ratio at 300°C and 500 bars for 7, 10.5, 17, 35, and 90 days, as described below.

Preparation and hydrothermal treatment of the gels

Gel preparation. Gels were prepared by combining a suspension of colloidal silica (Ludox) with solutions of K_2CO_3, $Al_2(NO_3)_3 \cdot 9H_2O$, $Fe(NH_4)_2(SO_4)_2 \cdot 6H_2O$, and Mg metal. Ludox and aluminum nitrate were standardized by ignition of aliquots of each at 800°C. Potassium carbonate was dried to constant weight before use. The required amounts of the above compounds for each gel composition were weighed into separate 50-ml beakers and covered with parafilm. Aluminum nitrate and ferrous ammonium sulfate were dissolved in distilled water; Mg metal and K_2CO_3 were dissolved in a solution of redistilled 3 M HNO_3.

Solutions containing the calculated amounts of source compounds were then placed in a 250-ml polyethylene bottle. The aluminum nitrate solution was mixed initially with the Mg or Fe solution, and the K_2CO_3 solution was then added slowly. Some precipitate formed at this point, but was dissolved with stirring and the addition of a few milliliters of concentrated HNO_3. The required amount of Ludox was added as a final step, and the bottle was placed on a stirring plate to allow the gel to form. The upper portion of the polyethylene bottles containing the gels was sliced off with a razor blade and covered with watch glasses. The gels were evaporated at low temperature until dry, transferred to Vycor crucibles, and heated in air to 800°C for 2 hr to convert them to glasses. The glass was ground to a fine powder and used as the starting materials in the gold capsules for the hydrothermal runs. This procedure completely oxidized ferrous compounds to ferric oxide in the Fe-bearing gel. Presumably, the iron remained

Table 1. Energy-dispersive X-ray (EDX) spectral analysis[1] of phyllosilicate standards.

Mineral	Spectral intensity ratios/Si				Atomic ratios/Si from EDX analysis				Atomic ratios/Si From bulk chemistry			
	Al	Mg	Fe	K	Al	Mg	Fe	K	Al	Mg	Fe	K
Wyoming montmorillonite	0.36	0.05	0.07	—	0.39	0.07	0.05	—	0.41	0.08	0.06	—
Silver Hill, Montana, illite	0.49	0.04	0.12	0.26	0.53	0.06	0.09	0.23	0.47	0.08	0.09	0.19
Georgia muscovite	0.79	0.03	0.03	0.34	0.86	0.04	0.02	0.30	0.88	0.02	0.04	0.30
Biotite	0.43	0.27	0.66	0.38	0.46	0.39	0.49	0.34	0.46	0.46	0.48	0.33
Talc	—	0.52	—	—	—	0.74	—	—	—	0.75	—	—
Pyrophyllite	0.52	—	—	—	0.57	—	—	—	0.57	—	—	—

[1] Also referred to as "X-ray microanalysis" elsewhere in text.

as the ferric ion during the course of the experiment because of the low permeability of gold capsules to hydrogen at 300°C of the experiments.

The starting glass fragments were examined by X-ray powder diffraction (XRD) and analytical electron microscopy (AEM). The glass fragments in all three gels consisted of minute granules having equant to irregular forms. X-ray microanalysis indicated that the glass fragments were not chemically homogeneous with respect to their Al/Si and K/Si atomic ratios. For example, the Al/Si atomic ratio ranged from 0.30 to 0.50 in the glass fragments of gel I, which was prepared to have an Al/Si ratio of 0.82. Similarly, the K/Si ratio of the glass fragments ranged from 0.10 to 0.22, as compared with 0.21 for the bulk gel. The glass powder in gels I and III was amorphous to X-rays; in Fe^{3+}-bearing gel II, part of the iron oxide was crystallized as hematite and part of the aluminum oxide as corundum. Hematite was identified by distinct XRD reflections at 2.68, 2.51, 2.20, 1.83, and 1.69 Å, and small amounts of corundum give rise to weak reflections at 2.39, 2.10, and 1.61 Å.

Hydrothermal experiments. The experiments were performed in cold-seal pressure vessels equipped with a rapid-quench device, using procedures similar to those reported by Huang *et al.* (1986). For each run, about 50 mg of solid glass powder and an equivalent amount of distilled water (1:1 solid/water ratio) were welded shut into a gold capsule 3.5 cm long and 20 mm in diameter. Sealed capsules containing the three illite gels were then loaded into a single pressure vessel to ensure that they would react under exactly the same conditions. No attempt was made to control the oxygen fugacity during the experiments. The pH of the initial and final quenched solutions could not be measured because of the high solid/fluid ratio and the small volume of the fluid; the pH was assumed to be close to neutral. The red color of the solid sample before and after the experiment indicated that the ferric iron predominated in solution during the experiment. Ultrapure argon was the pressure medium used. Pressures were accurate to ±5%, and temperatures were precise to ±5°C and accurate to better than ±10°C.

Characterization of reaction products

The reaction products were analyzed by XRD and AEM as described below.

X-ray powder diffraction analysis. Oriented mounts of the solid reaction products were prepared by ultrasonically dispersing a 10-mg sample in 0.5 ml of distilled water, followed by sedimentation onto a glass slide. Sample coverage within an area 19 mm × 19 mm provided 80% of "infinite thickness" at 20°2θ. XRD patterns were collected in Exxon Production Research Laboratory by one of us (W.L.H.) using a Siemens D-500 diffractometer equipped with a graphite (diffracted beam) monochromator and CuKα radiation. A fixed-slit assembly and 0.018° detector diaphragm (receiving slit) were used. Data were collected using a strip chart recorder. Goniometer and chart speeds, respectively, were 1°2θ/min and 1 cm/min.

Identification of the reaction products was based on XRD patterns of ethylene glycol-solvated clay slides. The nature of the I/S mixed-layering was determined by comparing the $(001)_{10Å}/(002)_{17Å}$ and $(002)_{10Å}/(003)_{17Å}$ peak positions with those calculated by Reynolds (1980), and by subsequently simulating the XRD patterns with the NEWMOD computer program (available from R. C. Reynolds, 8 Brook Drive, Hanover, New Hampshire).

Analytical electron microscopy. A JEM-100CX analytical electron microscope, operated at 100 kV potential, was used to examine the reaction products. Powders of the reaction products were first suspended in ultrapure distilled water to which trace amounts of tertiary butylamine had been added. A drop of the suspension was dried on a Cu grid covered with a Formvar film; the film was subsequently coated with C/Pt or C alone.

The chemical composition of the individual clay particles was determined using a KEVEX 8000 X-ray microanalyzer attached to the electron microscope column. The characteristic X-ray spectra generated by the elements of an individual clay crystallite were collected by an ultrathin window detector. A selected area of 0.5 square micrometers of a clay particle was scanned for 100 s at 100 kV potential to minimize K-migration under the electron beam. Energies of the characteristic X-ray photons were then differentiated by a multichannel analyzer and processed by an on-line computer using KEVEX's TEMSTAR software. The net spectral intensities (i.e., after correcting for the background) of an element (I_x) were then converted to atomic ratios ($N_{x/Si}$) by the relationship known as the thin-film approximation:

$$N_{(x/Si)} = k_{(X/Si)}(I_x/I_{Si}).$$

This relationship is valid as long as the thickness of the clay particles is <0.1 μm at 100-kV potential. The k-factors are obtained from the phyllosilicates of known chemical compositions; the k-factors for this study were derived from muscovite, phlogopite, and annite:

$k_{(Al/Si)} = 1.085$ (from phlogopite),
$k_{(K/Si)} = 0.888$ (from muscovite),
$k_{(Mg/Si)} = 1.411$ (from phlogopite),
$k_{(Fe/Si)} = 0.733$ (from annite).

Thin particles of Wyoming montmorillonite, Silver Hill illite, and Georgia muscovite were also analyzed under the above experimental conditions (Table 1). Ten particles from each sample were analyzed and the mean value was calculated. The relative standard errors of the measurements ranged from 10 to 20%, except for atomic ratios <5%. The discrepancies

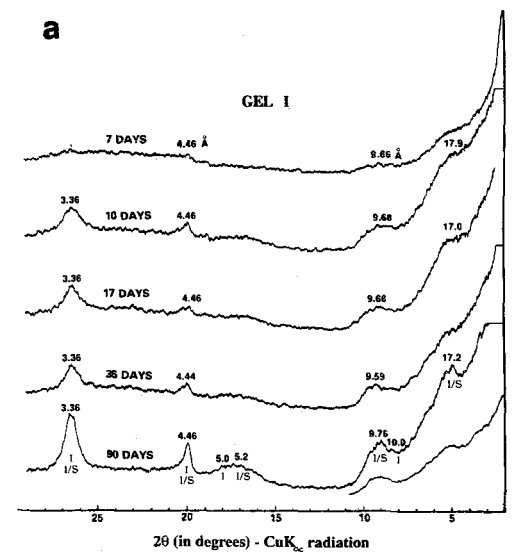

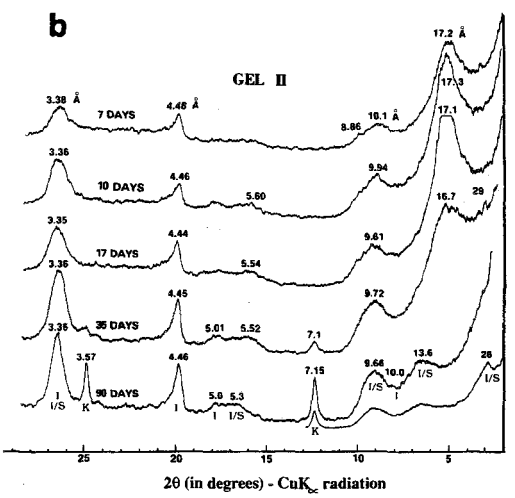

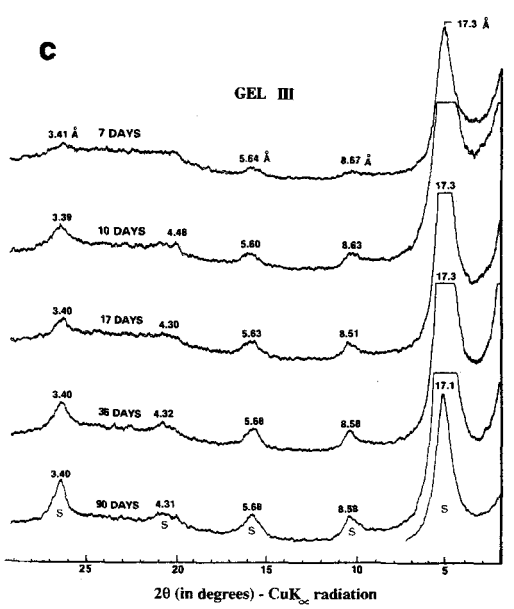

between the bulk chemical analysis and the X-ray microanalysis of the individual particles were mostly acceptable.

Similarly, the particles in the reaction products were analyzed by selecting 5–10 particles of a certain morphology (flakey aggregate, platelet, thin lath), and the average spectral intensities for each morphological type were calculated. These spectral intensities were then converted to atomic ratios with respect to Si using the above k-factors. Structural formulae of the clay particles were then derived from the atomic ratios assuming that the total number of octahedral and tetrahedral cations was equal to 6.0. Because the K readings were erroneous, the conventional 11-oxygen equivalency was not used.

RESULTS OF THE INVESTIGATIONS

The reaction products were identified by XRD and their morphological and chemical characteristics were determined by AEM.

Gel I, illitic composition having no octahedral substitutions

XRD patterns (Figure 1a) indicate that I/S was the only crystalline material in the reaction product. Three rather broad basal reflections were noticed in the XRD patterns from runs lasting as long as 35 days, indicating that only a small portion of the starting glass had crystallized. The prismatic, 02,11 reflections at 4.46 Å for I/S clays was rather strong relative to the intensities of the basal reflections, indicating that the clay particles were not highly oriented, although they were sedimented from a dispersion. This was found to be related to the fact that most of the clay crystallites were still edge-wise attached to the surface of the starting glass fragments, as shown in the scanning electron image in Figure 2a. Consequently, the basal reflections of the clays were broad and few in number. A broad reflection ranging from 8.9 to 10.1 Å and peaking at about 9.7 Å was the only peak available for determining the composition of the I/S. The peak position was not clearly distinguishable, and the derived expandability of the clay was not reliable. The 9.7-Å peak position and the broad low-angle shoulder at about 17 Å were comparable to a NEWMOD simulated pattern of a randomly interstratified I/S having 30% expandability. The non-expandable layers probably include K^+-saturated and highly charged smectite layers in the reaction products. The clay was not Na-saturated prior to XRD analysis because of the small quantities (30 mg) of the available sample.

The amount of the crystalline reaction products definitely increased in runs from 7 to 90 days. After 90 days, a $(002)_{17Å}/(001)_{10Å}$ peak appeared at 9.76 Å, and a weak $(003)_{17Å}/(002)_{10Å}$ reflection was distinguishable

←

Figure 1. X-ray powder diffraction patterns of reaction products from illitic gels treated at 300°C and 500 bars for 7–90 days; (a) gel I; (b) gel II; and (c) gel III. I = illite, S = smectite, and I/S = illite/smectite mixed-layer.

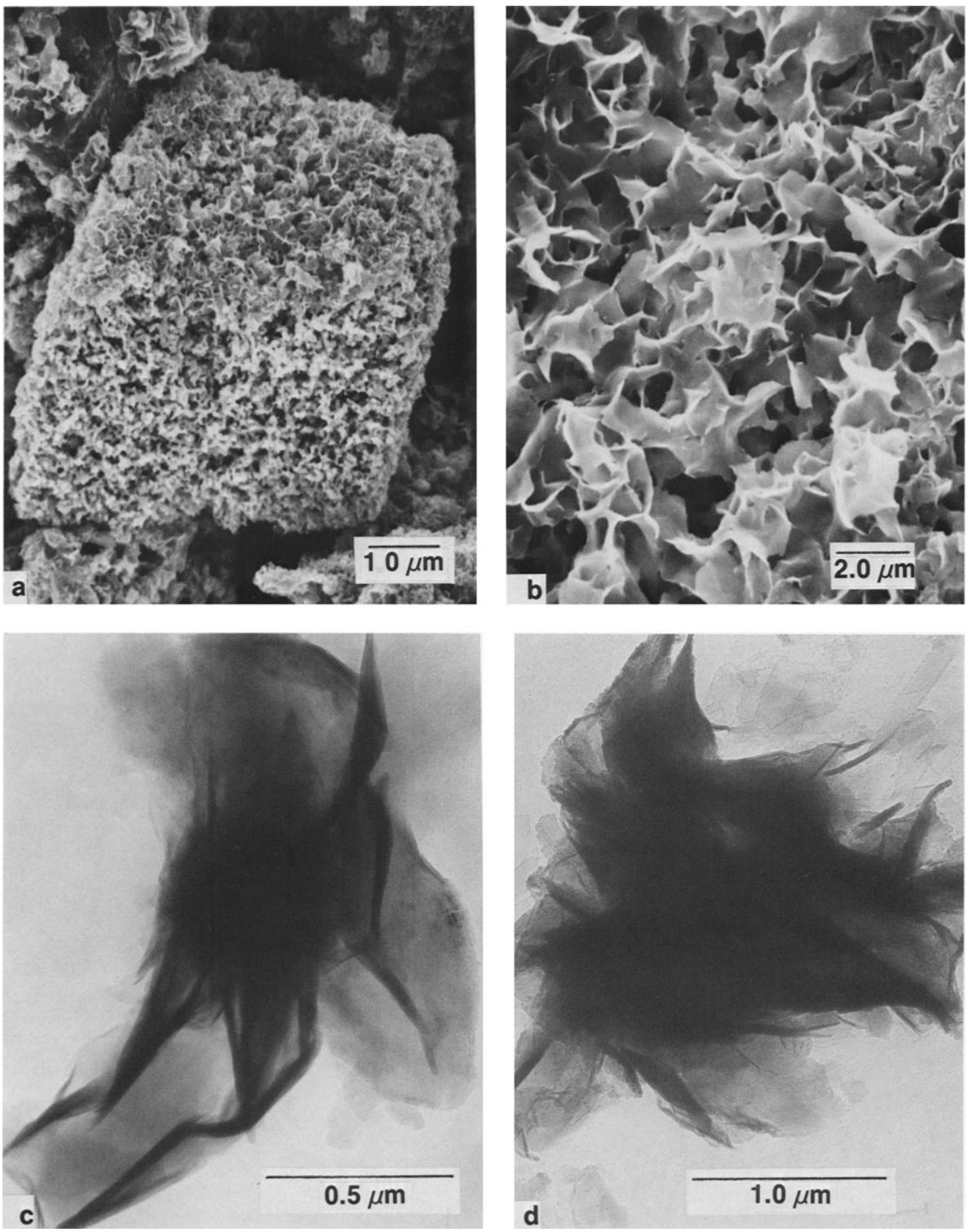

Figure 2. Scanning (SEM) and transmission electron (TEM) images of the illite/smectite (I/S) formed from gel I: (a) SEM of clay precipitates on glass fragments; (b) SEM of honeycombs made of I/S flakes in the clay precipitates; (c–d) TEMs of foliated aggregates of flakes having smectite morphology formed in 10.5- and 90-day runs.

https://doi.org/10.1346/CCMN.1991.0390408 Published online by Cambridge University Press

Table 2. Average atomic ratios obtained from X-ray microanalysis and structural formulae for illitic clay reaction products.

Reaction time (days)	Reaction product	Average atomic ratios/Si				Structural formulae					
						Tetrahedral		Octahedral			Inter-layer
		Al	Mg	Fe	K	Si	Al	Al	Mg	Fe	K
					Gel I						
7	I/S flake	0.67	—	—	0.11	3.59	0.41	2.00	—	—	0.39
10.5	I/S flake	0.62	—	—	0.14	3.70	0.30	2.00	—	—	0.52
10.5	I/S platelet	0.58	—	—	0.16	3.80	0.20	2.00	—	—	0.60
17	I/S flake	0.64	—	—	0.11	3.66	0.34	2.00	—	—	0.40
35	I/S flake	0.66	—	—	0.13	3.61	0.39	2.00	—	—	0.47
35	I/S platelet	0.67	—	—	0.15	3.59	0.41	2.00	—	—	0.54
90	I/S flake	0.68	—	—	0.10	3.57	0.43	2.00	—	—	0.36
90	I/S platelet	0.67	—	—	0.11	3.59	0.41	2.00	—	—	0.39
					Gel II						
7	I/S flake	0.61	—	0.07	0.12	3.57	0.43	1.75	—	0.25	0.43
10.5	I/S flake	0.62	—	0.07	0.10	3.55	0.45	1.75	—	0.25	0.36
17	I/S flake	0.62	—	0.07	0.10	3.55	0.45	1.75	—	0.25	0.36
17	I/S platelet	0.62	—	0.04	0.13	3.61	0.39	1.86	—	0.14	0.47
35	I/S flake	0.58	—	0.04	0.14	3.70	0.30	1.85	—	0.15	0.52
35	I/S ribbon	0.55	—	0.06	0.18	3.73	0.27	1.78	—	0.22	0.67
90	I/S flake	0.69	—	0.05	0.13	3.55	0.45	1.82	—	0.18	0.46
90	I/S platelet	0.64	—	0.03	0.13	3.59	0.41	1.89	—	0.11	0.46
					Wyoming montmorillonite						
Natural	S flake	0.39	0.07	0.05	—	3.97	0.03	1.55	0.29	0.20	—
					Silver Hill illite						
Natural	I platelet	0.53	0.06	0.09	0.23	3.66	0.34	1.38	0.29	0.33	0.70

I/S = illite/smectite; S = smectite; I = illite.

at 5.2 Å (Figure 1a). The 5.2-Å reflection was also broad, indicating a range of expandabilities and lateral domain sizes. Basically, the XRD patterns were similar in all the runs, suggesting that the mode of interstratification (R0) and the amount of expandability did not change noticeably within 90 days. The amount of the crystallization products definitely increased and their crystallinity slightly improved with time, as suggested by the sharpening and increasing intensities of the reflections. Two extremely weak reflections at 10.0 and 5.0 Å were also present in the XRD pattern of the 90-day run, which indicate the presence of discrete illite in very small quantities (<5%).

Scanning electron images of the reaction products show that glass fragments had been gradually covered by a clay coating that precipitated during the hydrothermal treatment (Figure 2a). Clay precipitates displayed a honeycomb texture consisting of curled flakes (Figure 2b). The morphological features of the individual clay particles in these honeycombs were examined by transmission electron microscopy and they appeared mainly in two distinct forms.

1. Foliated aggregates. Foliated aggregates having a dense core consisting of curled flakes, morphologically similar to smectite, were found in the runs from 7 to 90 days. Typical flakey aggregates are displayed in Figure 2c for the 10.5-day run and in Figure 2d for the 90-day run. In general, these foliated aggregates were 2–4 μm in size and were commonly surrounded by thin, platy (lamellar) overgrowths along their rims (Figures 3a and 3c for 10.5- and 90-day runs, respectively). A close view of the platy overgrowths (Figure 3d) illustrates minute platy domains ranging in size from 200 Å to 0.2 μm and ranging in shape from rhombohedral to rectangular. These thin platelets are locally broken and detached from the main aggregate and appear as individual thin platelets in the size range 0.1–0.7 μm. They have euhedral to anhedral outlines, as shown in the background of Figure 3a for the 10.5-day run. X-ray microanalysis of the platelets and dense flakey aggregates are summarized in Table 2. Excluding platelets in the 10.5-day run, similar Al/Si and K/Si ratios were obtained from the flakey aggregates and thin platelets, including the above-mentioned overgrowths in all runs. No significant chemical differences were found between the platy rims and the dense curly cores.

2. Compact plates. Compact platy particles and their aggregates consisting of thicker platelets that showed no folding or curling of thin films were noted in the 7- to 90-day runs. They ranged in size from 0.2 to 2.0 μm. A typical platelet is displayed in Figure 3b for the 10.5-day run. These platelets show no regular forms (outlines) and have Al/Si and K/Si ratios similar to the flakey aggregates, as mentioned above.

Two types of aggregates (foliated and compact platy) were the most common reaction products in the runs; they represented randomly interstratified I/S, as iden-

https://doi.org/10.1346/CCMN.1991.0390408 Published online by Cambridge University Press

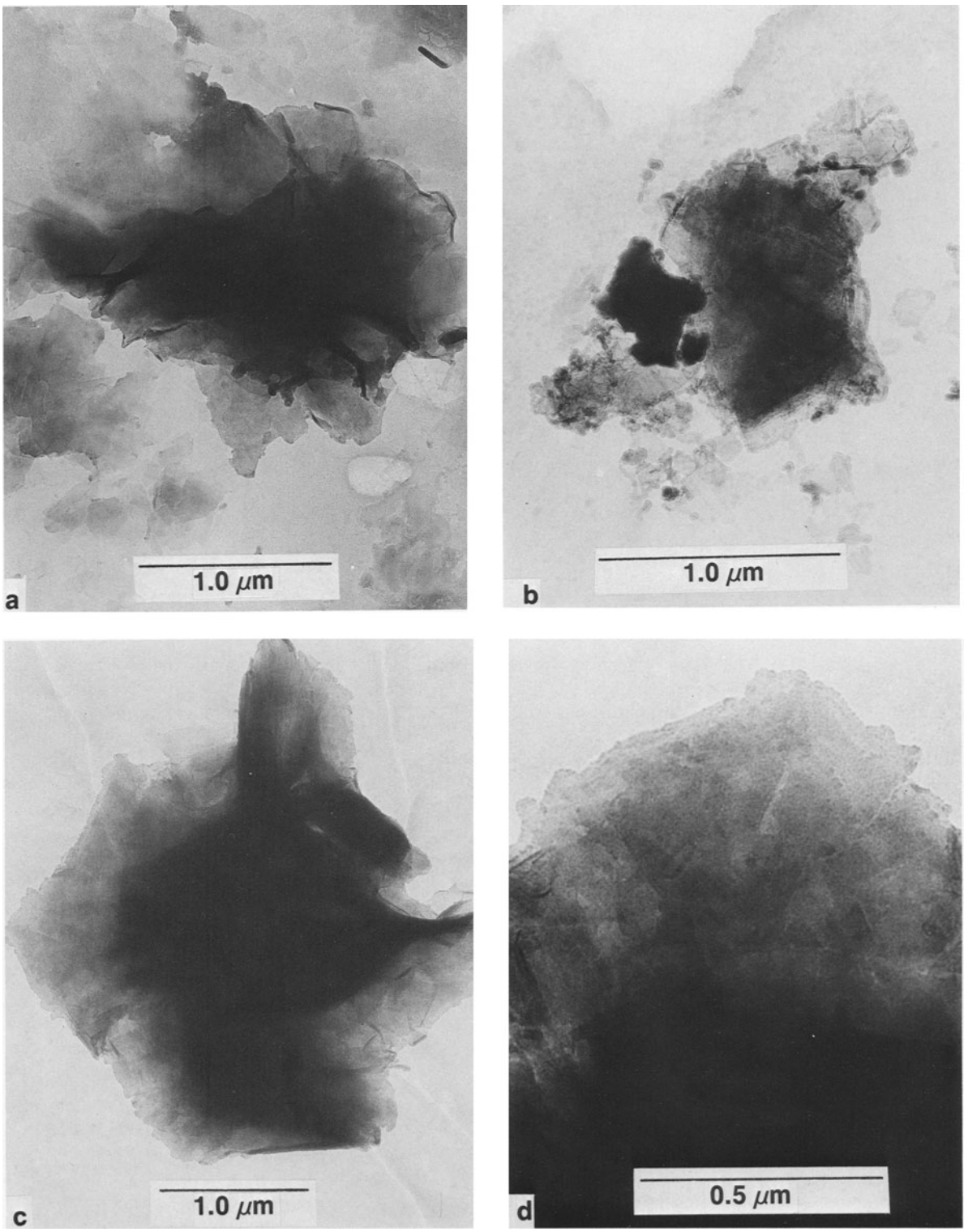

Figure 3. Transmission electron images of the interstratified illite/smectite (I/S) formed from gel I: (a) foliated flakes of I/S with platy overgrowths and thin, subhedral to euhedral platelets in the background; (b) thick platelet of I/S; (c) clay particle showing a dense core of foliated flakes having smectite-like morphology and subsequent platy overgrowths along the rims of flakes; and (d) high-magnification view of overgrowth showing a mosaic of thin, platy domains.

https://doi.org/10.1346/CCMN.1991.0390408 Published online by Cambridge University Press

tified by XRD. From the data listed in Table 2, the smectite layers in flakes and platelets are obviously beidellitic, carrying tetrahedral layer charges. The atomic Al/Si ratios of the flakes and platelets ranged from 0.62 to 0.68, comparable to the ratio of (Al + Fe + Mg)/Si in the Silver Hill illite. The atomic K/Si ratios of the above flakes ranged from 0.10 to 0.14, compared with 0.23 for the Silver Hill illite and 0.34 for the Georgia muscovite (Tables 1 and 2). Similar atomic Al/Si and K/Si ratios were found for the platelets, except for those formed in the 10.5-day runs; here, the Al/Si ratio was 0.58 and the K/Si ratio was 0.16. The structural formulae for the flakey and platy I/S randomly interstratified in these products indicate average layer charges ranging from 0.30 to 0.43 and interlayer potassium contents ranging from 0.36 to 0.52 (with one exception, as indicated in Table 2). The K content of the products were not as uniform as the Al content in the I/S and commonly not in agreement with the layer charge.

A significant morphology of illitic reaction products consisted of thin laths and their lattice-like (reticulated) arrangements, which were found in small amounts after 35 and 90 days of ageing. Due to their small quantities, XRD determination of the interstratification mode in these laths was not possible. As shown in Figure 4a, these laths are as long as 2.0 μm, as wide as 0.05–0.1 μm, and only a few layers thick. These thin laths are commonly arranged in a meshwork consisting of sets 120° apart, giving rise to selected-area electron diffraction patterns having distinct spots like a single crystal (Figure 4b). Denser platy or irregular cores in the center of the meshwork of laths were also noted. Euhedral hexagonal platelets of illite seem to have formed by lattice-like coalescence of laths, rhombs, and triangular-shaped domains (Figures 4c and 4d).

Gel II, illitic composition having Fe^{3+}-octahedral substitutions

XRD patterns of the reaction products of gel II indicate that large amounts of crystalline material consisting of I/S formed in these runs (Figure 1b). The prismatic 02,11 reflections of the clays at 4.45–4.48 Å were here also rather prominent, indicating that the clay particles were not highly oriented, for the reasons mentioned previously. The patterns of products of runs of 7–17-days duration showed a strong 17-Å reflection and a broad $(002)_{17Å}/(001)_{10Å}$ reflection in the range 8.9–10.1 Å, with ill-defined maxima. A weak $(003)_{17Å}/(002)_{10Å}$ reflection was present at 5.60 Å after 10.5 days, at 5.54 Å after 17, at 5.52 Å after 35 days, and at 5.3 Å after 90 days. The positions of the $(003)_{17Å}/(002)_{10Å}$ reflection suggest that the I/S contained about 10% illite after 10.5 days and 35% illite after 35 days. The XRD pattern of the 90-day run was completely different from the others; the illite content of the I/S increased to 75%, as indicated by the spacing of the $(003)_{17Å}/(002)_{10Å}$ reflection (5.3 Å). Moreover, superlattice reflections at 28 and 13.6 Å were present; the simulated XRD pattern suggests that the I/S mixed-layer was now R1 ordered.

Weak but discernable reflections at 10.0 and 5.00 Å indicate the presence of small amounts (<5%) of discrete illite in the 35- and 90-day runs. In addition, small amounts of kaolinite were identified in these runs by the presence of 7.15- and 3.57-Å reflections.

Electron microscopic examination of the products in the 7–17-day runs indicated that randomly interstratified I/S predominantly formed both as foliated aggregates and as compact platelets. As shown in Figure 5c, the foliated aggregates are composed of curled flakes having a dense core and are surrounded by overgrowths of thin platelets. The foliated aggregates are similar in morphology to smectite and range in size from 1 to 4 μm. In these aggregates the denser core is composed of curled and foliated thin films. Thin platelets are common as overgrowths along the rims of the dense aggregates (Figure 5d); some display perfect rhombohedral forms in the size range 0.5–1.0 μm. The growth relationship between the smectite-like irregular cores and the platy overgrowths is discernable in Figures 5a and 5b. The rhomb-shaped overgrowths display a microstructure consisting of two sets of fine laths 120° apart, which appear to have grown along the edges as an extension of the flakes. Dense foliated cores appear to consist of smectite-rich I/S with smectite segregation, and the platy overgrowths appear to represent illite segregation; however, the X-ray spectral data in Table 2 show no significant chemical differences between the foliated cores and platy rims in these I/S aggregates. The Al/Si atomic ratios in the flakes or platelets of randomly interstratified I/S formed within 7–35-day range from 0.58 to 0.62, whereas the K/Si ratios range from 0.10 to 0.14 (Table 2). These variations are just within the standard deviations of the measurements.

A morphologically different phase was observed in small amounts in the reaction products of the 35-day run. It occurred as a stack of ribbons (Figures 6a and 6b). The ribbons were typically 0.1 μm wide and about 2.0 μm long. They displayed Moiré fringes (Figure 6b), indicating that the ribbons were slightly displaced with respect to each other. The K/Si atomic ratio was found to be 0.18 ± 0.02 for these ribbons, and Al/Si and Fe/Si ratios were found to be 0.55 ± 0.03 and 0.06 ± 0.02, respectively. These ribbons were more prominent in the 90-day run.

R1-ordered I/S, having a 25% expandability after the 90-day run, occurred as aggregates of euhedral platelets having regular outlines (mostly rhomb-like) and ribbons (elongated lamellae) as large as 1.0 μm (Figure 6c and 6d). The atomic ratios of these ribbons and thicker lamellae having better developed crystallite

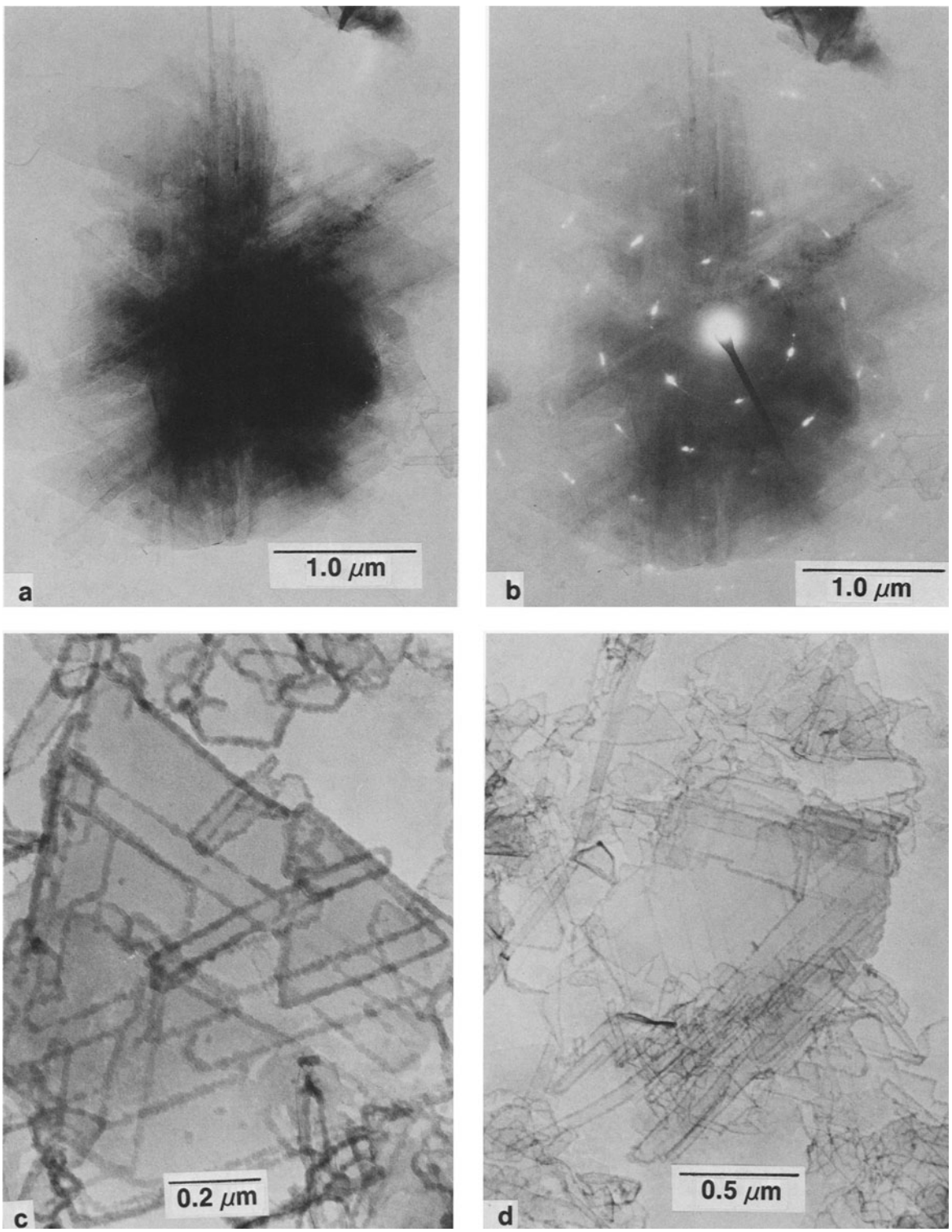

Figure 4. Transmission electron images of illite/smectite (I/S) particles of unusual morphology and texture formed in small quantities from gel I after 35 days: (a) laths of I/S arranged in three sets 120° apart; (b) selected-area electron diffraction pattern of meshwork of laths in Figure 4a; and (c–d) laths, rhombs, and triangular islands in an euhedral illite platelet.

https://doi.org/10.1346/CCMN.1991.0390408 Published online by Cambridge University Press

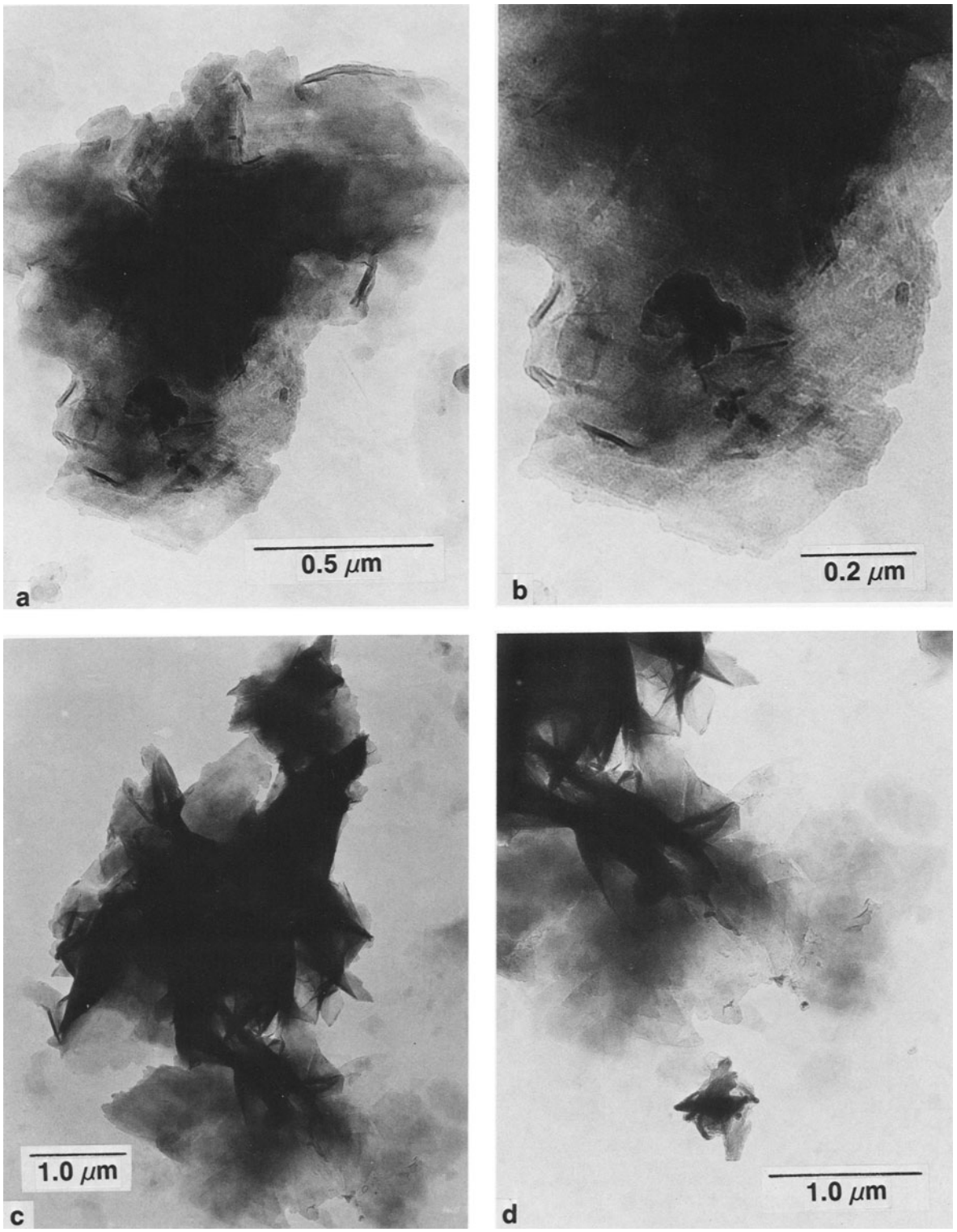

Figure 5. Transmission electron images of typical illite/smectite (I/S) particles from Fe^{3+}-bearing gel II treated at 300°C and 500 bars: (a) I/S particle showing dense core of irregular flakes and platy overgrowths having euhedral forms; (b) high-magnification view of platy overgrowth displaying a microstructure consisting of two sets of fine laths 120° apart; (c) typical aggregate of foliated flakes having smectite morphology and platy overgrowths; and (d) high-magnification view of overgrowths, occurring mostly as thin hexagonal or rhomb-shaped platelets.

https://doi.org/10.1346/CCMN.1991.0390408 Published online by Cambridge University Press

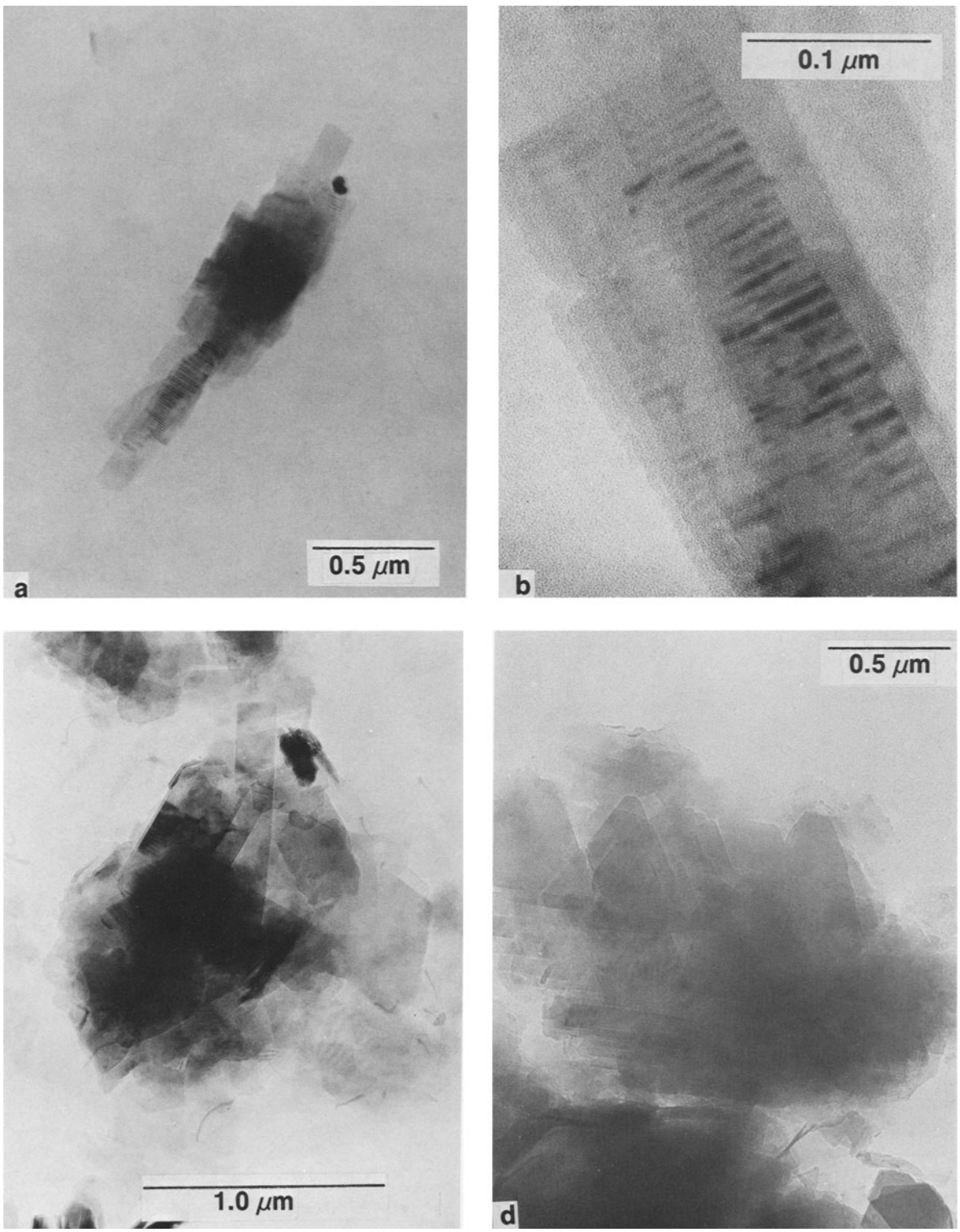

Figure 6. Transmission electron images of illite/smectite (I/S) reaction products of Fe^{3+}-bearing gel II showing euhedral crystal forms: (a) stack of ribbons of I/S formed in 35-day runs; (b) high-magnification view of ribbons displaying Moiré fringes; and (c–d) ribbon-like and hexagonal particles that formed in 90-day run.

https://doi.org/10.1346/CCMN.1991.0390408 Published online by Cambridge University Press

Figure 7. Transmission electron images of foliated aggregate of smectite flakes formed from Mg^{2+}-bearing gel on reacting at 300°C and 500 bars for 35 days.

forms were 0.66 ± 0.03 for Al/Si, 0.11 ± 0.02 for K/Si, and 0.04 ± 0.02 for Fe/Si.

Gel III, illitic composition having Mg^{2+}-octahedral substitutions

The XRD patterns of the reaction products of gel III in Figure 1c show the presence of a 100% expandable smectite as the only product in all runs from 7 to 90 days. The amount of smectite and its degree of crystallinity seem to have increased appreciably from 7 to 90 days, as evidenced by both the intensity and the sharpness of the smectite reflections, which significantly increased with time. No illite layers were apparently formed from the Mg^{2+}-bearing illitic gel.

Clay particles in products from this gel consisted of large foliated aggregates of folded films and wrinkled flakes (Figure 7), as large as 4 μm. These aggregates were morphologically similar to the smectite that is common in Wyoming bentonite. In all these smectite aggregates, the central (core) section was dense and contained excessively curled films, whereas the rims consisted of thin and lamellar (platy) forms. Similar thin lamellae were detached from the aggregates and occurred as individual platelets. The morphological features of the smectites formed in the 90-day run were somewhat different from those crystallized in 7–35-day runs. The smectite aggregates in the 90-day run were more compact and less foliated. They consisted of platy units having anhedral forms with irregular outlines, but without the curled films and wrinkled flakes.

INTERPRETATION OF THE RESULTS AND CONCLUSIONS

Experimental alteration of the synthetic glasses of the present investigation involved two major complications that must be kept in mind while interpreting the results:

1. The chemistry of glass particles was inhomogeneous and had less Al, Fe, and K than the starting gel. Some of the iron and alumina segregated as hematite and corundum. Thus, the chemical compositions of the clays were significantly different from those of the starting gels. The deficiencies in Al and K were possibly responsible for the fact that the illitization reactions were not fully realized and were limited to the formation of I/S.
2. The starting glass was not completely altered in the experiments. While the residual glass was reacting to smectite, the early-formed smectite was converting to illite.

Although the extent of octahedral substitutions in I/S products was less than in the starting gels, the effects of these substitutions on morphology and mode of interstratification were still significant, as described below.

Illitic clays having no octahedral substitutions

After hydrothermal treatment at 300°C and 500 bars for 7 to 90 days, the illitic gel containing no Mg^{2+} and Fe^{3+} yielded clays having randomly interstratified I/S and 30%(?) or more expandability. The illite content and the chemical composition (Al/Si, K/Si ratios) of the mode of I/S interstratification remained essentially constant regardless of the duration of the experiments (7–90 days). The randomly interstratified I/S was found predominantly as foliated aggregates of curled flakes, morphologically similar to smectite. These flakey aggregates probably represent the initial precipitation of I/S from a highly supersaturated solution. The flakey aggregates were commonly surrounded by overgrowths at their edges, consisting of thin platelets, which may have formed at lower supersaturations at a later stage. The thin platy overgrowths were locally detached from the aggregates and occurred as individual lamellae in the size range 0.2–0.5 μm.

A few illitic particles having an unusual morphology formed in samples reacted for 35 and 90 days as thin laths, commonly in lattice-like arrangements (reticu-

https://doi.org/10.1346/CCMN.1991.0390408 Published online by Cambridge University Press

lations). These laths were as long as 4–5 μm and were morphologically similar to the "fibrous illite" found in many diagenetic products. The lath-like units in this study were, however, similar in chemical composition to the flakey, smectite-like aggregates. The laths formed in a rather simple chemical system—aluminous illitic gel containing no Fe^{3+} and Mg^{2+}. Gels reacted for 90 days under the same experimental conditions led to greater yields of crystallized I/S having essentially the same chemical composition, the same amount of expandability (30%), and the same mode of interstratification (R0). The chemical compositions and interstratification sequence of the reaction products seem to have been determined by the chemistry of the system at 300°C and to have underwent no significant evolution with time within 90 days. The crystallization of lath-shaped and platy I/S particles appears to have proceeded by edge-wise overgrowth; no spiral growth was observed in the reaction products. With reference to the crystal structure of 1 M mica, the laths are parallel to [100], [$\bar{1}$10], and [$\bar{1}\bar{1}$0], the directions of the chains of silicate tetrahedra within the tetrahedral sheets and the chains of alumina octehedra within the octahedral sheets. In other words, these are the growth directions of broken bonds at the edges of layers, along which no nucleation or no spiral growth step are needed (see Grim and Güven, 1978, for details). The lath-like units are morphologically similar to "fibrous" illites that have been found as diagenetic products in reservoir sandstones, see, e.g., Güven *et al.*, 1980; McHardy *et al.*, 1982; Huggett, 1982; Pallatt *et al.*, 1984. The average atomic ratios of Al/Si and K/Si in the above thin laths are 0.66 ± 0.03 and 0.14 ± 0.02, respectively; these ratios are close to those found for the flakey aggregates having smectite morphology in the same runs.

Role of Fe^{3+} in hydrothermal illitization

The addition of small amounts of Fe^{3+} into the starting gel greatly enhanced the crystallization rate, improved the morphology and the order of interstratification, and yielded larger amounts of I/S. The chemical composition of the illitic clays showed no significant variations with reaction time within 90 days. The expandability of the I/S reached 65% within 35 days and was reduced to 25% after 90 days. The randomly interstratified I/S in runs of 7–35 days were predominantly in the form of smectite-like foliated aggregates surrounded by overgrowths of mostly euhedral platelets. The mode of interstratification was found by XRD to have changed from random (R0) to regular (R1) after 90 days. The regularly interstratified I/S which formed after 90 days displayed a different morphology, consisting of ribbons and thicker lamellae having regular (rhombohedral) forms. The I/S having ribbon-like morphology appeared first after 35 days of ageing, but in rather small quantities.

The role of Mg^{2+} in hydrothermal illitization

Mg^{2+}, on the other hand, dramatically inhibited the formation of illitic layers and favored the crystallization of smectite. This is consistent with previous investigations on the role of Mg^{2+} in the conversion of smectite to illite (Eberl, 1978a; Roberson and Lahann, 1981).

Hydrothermal illitization of volcanic glass in nature

Hydrothermal illitization of volcanic glass in nature has been described in numerous publications, but Inoue and Utada (1983) and Inoue *et al.* (1978, 1987, 1988) demonstrated the entire spectrum of smectite-to-illite conversion at a single location. These investigators found that silicic volcanic tuffs (glasses) were altered to various degrees within a few hundred meters from the margin to the center of a hydrothermal field in the Shinzan area of Japan. Here pure smectite having a 100% expandability occurs at the margin, and the expendability gradually decreases to 0% in the center of the hydrothermal field. The morphological and structural evolution of hydrothermal I/S phases were illustrated and two distinct stages were noted:

Stage 1. Pure smectites having 100% expandability displayed a flakey morphology of curled thin films and maintained this habit until the expandability was reduced to about 55%. The reduction of expandability was ascribed to the collapse of smectite layers by K-fixation, and the mode of interstratification was found to be random.

Stage 2. Neoformation of illite was thought to have taken place in three steps: dissolution of smectite, nucleation of illite, and growth of illite according to "Ostwald ripening" process. The neoformed illites were found to occur as laths and hexagonal platelets.

The experimental alteration of glass under hydrothermal conditions produced I/S phases that were remarkably similar in morphology and structure to those in the Shinzan area of Japan.

ACKNOWLEDGMENTS

Special thanks are due to G. A. Otten and K. C. Voight of Exxon Production Research Company, Houston, Texas, and to L. J. Lee, C. R. Landis, S. Sivalingam, and T. Schaef of Texas Tech University for their assistance during the experimental and data collection phases of the study. We thank J. M. Longo and D. R. Pevear of Exxon Production Research Company for valuable discussion throughout the study and for a review of an earlier version of this manuscript. The authors also thank G. Whitney and A. Inoue for their reviews, which considerably improved the manu-

script. We express our sincere appreciation to Kaylyn Dowdy for her patience in meticulously typing several versions of the manuscript.

REFERENCES

Eberl, D. (1978a) The reaction of montmorillonite to mixed-layer clay: The effect of interlayer alkali and alkaline earth cations: *Geochim. Cosmochim. Acta* **42,** 1–7.

Eberl, D. (1978b) Reaction series for dioctahedral smectites: *Clays & Clay Minerals* **26,** 327–340.

Eberl, D. and Hower, J. (1977) The hydrothermal transformation of sodium and potassium smectite into mixed-layer clay: *Clays & Clay Minerals* **25,** 215–227.

Grim, R. E. and Güven, N. (1978) *Bentonites: Geology, Mineralogy, Properties and Uses:* Elsevier, New York, 256 pp.

Güven, N., Hower, W. F., and Davies, D. K. (1980) Nature of authigenic illite in sandstone reservoirs: *J. Sed. Petrol.* **50,** 761–766.

Huang, W. L., Bishop, A. M., and Brown, R. W. (1986) The effect of fluid/rock ratio on feldspar dissolution and illite formation under reservoir conditions: *Clay Miner.* **21,** 585–601.

Huggett, J. M. (1982) On the nature of fibrous illite as observed by electron microscopy: *Clay Miner.* **17,** 433–442.

Inoue, A. (1983) Potassium fixation by clay minerals during hydrothermal treatment. *Clays & Clay Minerals* **31,** 81–91.

Inoue, A., Kohyama, N., Kitagawa, R., and Watanabe, T. (1987) Chemical and morphological evidence for the conversion of smectite to illite: *Clays & Clay Minerals* **35,** 111–120.

Inoue, A., Minato, H., and Utada, M. (1978) Mineralogical properties and occurrence of illite/montmorillonite mixed-layer minerals from Miocene volcanic glass in Waga-Omono district: *Clay Sci.* **5,** 123–136.

Inoue, A. and Utada, M. (1983) Further investigations of a conversion series of dioctahedral mica/smectites in the Shinzan hydrothermal alteration area, northeast Japan: *Clays & Clay Minerals* **31,** 401–412.

Inoue, A., Velde, B., Meunier, A., and Touchard, G. (1988) Mechanism of illite formation during smectite-to-illite conversion in a hydrothermal system: *Amer. Mineral.* **73,** 1325–1334.

McHardy, W. J., Wilson, M. J., and Tait, J. M. (1982) Electron microscope and X-ray diffraction studies of filamentous illitic clay from sandstones of the Magnus Field: *Clay Miner.* **17,** 23–40.

Pallatt, N., Wilson, M. J., and McHardy, M. J. (1984) The relationship between permeability and the morphology of diagenetic illite in reservoir rocks: *J. Petroleum Tech.* **36,** 2225–2227.

Reynolds, R. C. (1980) Interstratified clay minerals: in *Crystal Structures of Clay Minerals and their X-ray Identification:* G. W. Brindley and G. Brown, eds. Mineralogical Society, London, 249–303.

Roberson, H. E. and Lahann, R. W. (1981) Smectite-to-illite conversion rates: Effects of solution chemistry: *Clays & Clay Minerals* **29,** 129–135.

Whitney, G. and Northrop, H. R. (1988) Experimental investigation of the smectite to illite reaction: Dual reaction mechanisms and oxygen-isotope systematics: *Amer. Mineral.* **73,** 77–80.

(Received 2 May 1990; accepted 25 April 1991; Ms. 2010)